Electrochemical properties of Fe2O3-Nano-Loaded Carbon and Fe2O3-Nano/Carbon Mixed Composites for Iron-Air Battery Anodes

Hang, Bui Thi
Department of Applied Science for Electronics and Materials, Graduate School of Engineering Science, Kyushu University

Egashira, Minato
Faculty of Engineering, Yamaguchi University | Department of Applied Science for Electronics and Materials, Graduate School of Engineering Science, Kyushu University

Watanabe, Izumi
Institute for Materials Chemistry and Engineering

Hata, Satoshi
Department of Applied Science for Electronics and Materials, Graduate School of Engineering Science, Kyushu University

他

https://doi.org/10.15017/16756

出版情報：九州大学大学院総合理工学報告. 27 (1), pp.1-8, 2005-06. 九州大学大学院総合理工学府
バージョン：
権利関係：

九州大学大学院総合理工学報告
第27巻 第1号 1-8頁 平成17年6月

Engineering Sciences Reports, Kyushu University
(KYUSHU DAIGAKU SOGORIKOGAKU HOKOKU)
Vol. 27, No.1 pp.1–8 JUNE 2005

Electrochemical properties of Fe_2O_3-Nano-Loaded Carbon and Fe_2O_3-Nano/Carbon Mixed Composites for Iron-Air Battery Anodes

Bui Thi HANG[*1,†], Minato EGASHIRA[*2,*3], Izumi WATANABE[*2], Satoshi HATA[*1], Shigeto OKADA[*2], Jun-ichi YAMAKI[*2] and Seong-Ho YOON[*2]

†E-mail of corresponding author: *hang@cm.kyushu-u.ac.jp*

(Received May 11, 2005)

In order to find the adequate material for Fe/air battery anode, two kinds of materials, Fe_2O_3-nano-loaded carbon and Fe_2O_3-nano mixed carbon material using various carbon materials, were prepared. The Fe_2O_3-nano-loaded carbon material was prepared by loading Fe_2O_3 on carbon using a chemical method. $Fe(NO_3)_3$ was impregnated on carbon with different weight ratios of iron to carbon in an aqueous solution, and the mixture was dried and then calcined for 1 h at 400°C in flowing Ar. For the Fe_2O_3-nano mixed carbon material, Fe_2O_3-nano powder was mixed with carbon by mechanical method. The effect of various carbons on the physical and electrochemical properties of both Fe_2O_3-nano-loaded carbon and Fe_2O_3-nano mixed carbon electrodes was investigated and compared using X-ray diffraction (XRD), transmission electron microscopy (TEM), scanning electron microscopy (SEM) along with X-ray energy-dispersive spectroscopy (EDS), cyclic voltammetry (CV) and galvanostatic cycling performance. Transmission electron microscopy (TEM) coupled with X-ray diffraction measurements revealed that Fe_2O_3-nano particles were distributed on the carbon surface for Fe_2O_3-nano-loaded carbon. This distribution is similar to that for Fe_2O_3-nano mixed carbon electrodes observed by SEM and EDS. The CV results indicated that the redox currents of the Fe_2O_3-nano-loaded carbon are larger than that of correspondence Fe_2O_3-nano mixed carbon. Such properties are expected to provide the larger capacity for Fe_2O_3-nano-loaded carbon electrode than Fe_2O_3-nano mixed carbon electrode.

Key words: *Nano-carbon, Fe_2O_3-nano-loaded carbon, Fe_2O_3-nano mixed carbon, iron-air battery anode*

1. Introduction

High energy density for metal/air batteries has been the focus of attention in recent years for applications involving electric vehicles, among others [1-3]. The anode in an air battery plays a key role in deciding the performance, especially the specific capacity and cycle life. Iron is a potential candidate for metal/air battery anode. It is attractive material not only used in iron/air battery but also used in nickel/iron battery because high theoretical energy (0.96 Ah/g) and low cost [4-7, 15]. Thus, in recent years, iron electrodes have received considerable attention [4-16].

The overall electrochemical behavior involved in the passivation and dissolution of iron in alkaline solution was proposed earlier [4-5, 8-10, 11-13] containing two main steps, the first of which:

$$Fe + 2OH^- \rightleftarrows Fe(OH)_2 + 2e \quad (1)$$

(E^0 =-0.978 V vs. Hg/HgO [5])

According to some authors [10-11, 13], eqn. (1) involves the following partial steps in conjunction with the adsorption of OH^- ion:

$$Fe + OH^- \rightleftarrows [Fe(OH)]_{ad} + e \quad (2)$$

$$[Fe(OH)]_{ad} + OH^- \rightleftarrows Fe(OH)_2 + e \quad (3)$$

Most authors agree that the formation of $Fe(OH)_2$ proceeds through the formation of intermediate soluble species $HFeO_2^-$ [4-5, 8-9,

*1 Interdisciplinary Graduate School of Engineering Sciences, Department of Applied Science for Electronics & Materials
*2 Institute for Materials Chemistry and Engineering
*3 Present address (Faculty of Engineering, Yamaguchi University)

13-14], whose concentration is strongly temperature dependent [10-11], i.e.,

$$[Fe(OH)]_{ad} + 2OH^- \rightleftarrows HFeO_2^- + H_2O + e \quad (4)$$

and $$HFeO_2^- + H_2O \rightleftarrows Fe(OH)_2 + OH^- \quad (5)$$

The second oxidation step of iron electrode involves:

$$Fe(OH)_2 + OH^- \rightleftarrows FeOOH + H_2O + e \quad (6)$$
(E^0 = -0.658 V vs. Hg/HgO [5])

and/or

$$3Fe(OH)_2 + 2OH^- \rightleftarrows Fe_3O_4.4H_2O + 2e \quad (7)$$
(E^0 = -0.758 V vs Hg/HgO [12-13])

However, the problem of iron electrode is the a passive layer of $Fe(OH)_2$ formed during the cycling leading to a low utilization coefficient. Further, the potential of the Fe/ $Fe(OH)_2$ couple is only slightly more negative than that of the hydrogen evolution potential in alkaline solution [5, 7] thereby there is a simultaneous evolution of hydrogen evolution during charging [15-16], i.e.,

$$Fe + 2OH^- \rightleftarrows Fe(OH)_2 + 2e \quad (1)$$
(E^0 = -0.978 V vs. Hg/HgO)

and $$2H_2O + 2e \rightleftarrows H_2 + 2OH^- \quad (8)$$
(E^0 = -0.928 V vs. Hg/HgO)

This is the cause of the low charge/discharge efficiency and high self-discharge rate of iron electrode. In order to overcome the limitations of the iron electrode, a number of additives are incorporated in the iron electrode during fabrication [6, 11-12, 15-16] or in electrolyte [6, 11-14] or both [6, 11-12]. Recently, the authors reported that the Fe/carbon mixed composite electrodes, using various kinds of carbons as additives, showed improved the passivation, charge-discharge performance of the iron electrode [17]. However, in preparing such composite materials, it is preferable that the contact between iron and carbon be maximized. In order to increase the active material surface area, in the present study, we prepare two kinds of materials, Fe_2O_3-nano-loaded carbon and Fe_2O_3-nano mixed carbon, using various carbon materials, for use as an anode in Fe/air batteries.

2. Experiment

Vapor-grown carbon fibers (VGCF; Showa Denko Co.), acetylene black (AB, Denki Kagaku Co.) and natural graphite (Chuetsu Graphite Co.), with average diameters of ca. 200 nm, 100 nm and 18 μm, respectively, were used in the present work. In addition, two kinds of carbon nanofibers (CNFs), of the nanotube type, having an average diameter of ca. 50 nm, and a platelet type, having an average diameter of ca. 150 nm, were also investigated. For tubular CNF, hexagonal planes compose hollow tubes, while in platelet CNF, a smaller hexagonal plane is stacked perpendicular to the fiber axis. The main characteristics of the carbon materials employed are listed in Table 1 and their morphology is shown in Fig. 1. Iron nitrate (Wako Pure Chemical, Co.) was used as the iron source for Fe_2O_3-nano-loaded carbon while Fe_2O_3-nano powder (Aldrich) with average diameters of ca. 2-3 nm was used for Fe_2O_3-nano mixed carbon.

The Fe_2O_3-nano-loaded carbon material was prepared by loading Fe_2O_3 on carbon, as described below. $Fe(NO_3)_3$ was impregnated on carbon with various weight ratios of iron to

Table 1 Main characteristics of the carbon materials

	Grain size (nm)	BET surface area ($m^2 g^{-1}$)	True density ($g cm^{-3}$)
VGCF	100 ~ 300	13	2.21
AB	40 ~ 100	68	2.0
Natural graphite	18000	8	2.24
Tubular CNF	20 ~ 100	92	2.09
Platelet CNF	40 ~ 200	91	2.10

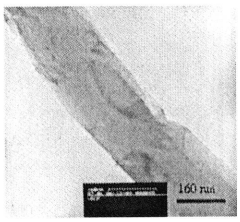

TEM image of VGC

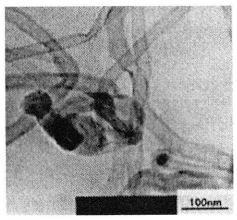

TEM image of tubular CNF

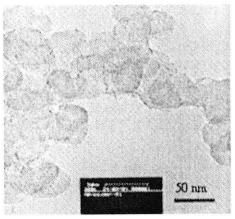

TEM image of AB

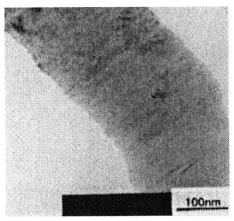

TEM image of platelet CNF

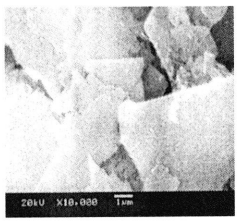

SEM image of graphite

Fig. 1 Morphology of carbon materials

carbon (1:1 and 1:8) in an aqueous solution, and the mixture was dried at 70°C, followed by calcination for 1 h at 400°C in flowing Ar. The iron compound obtained on the carbons was identified to be Fe_2O_3 by X-ray diffraction. The morphology of the as-prepared Fe_2O_3-nano-loaded carbon materials was observed by transmission electron microscopy (TEM), and scanning electron microscopy (SEM) together with X-ray energy dispersive spectroscopy (EDS). X-ray measurements were also carried out on these materials.

In order to obtain the electrochemical behavior of each Fe_2O_3-nano-loaded carbon and Fe_2O_3-nano mixed carbon material, two kinds of correspondence electrode sheet were prepared. For Fe_2O_3-nano-loaded carbon material, an electrode sheet was prepared by mixing 90 wt% of the respective Fe_2O_3-nano-loaded carbons and 10 wt.% polytetrafluoroethylene (PTFE; Daikin Co.) and rolling. In the case of Fe_2O_3-nano mixed carbon, which had two components, Fe_2O_3-nano powder (Aldrich), carbon and PTFE was mixed with the ratio of 45:45:10 wt. % and 10:80:10 wt.% to prepare electrode sheet by the same method. Both Fe_2O_3-nano-loaded carbon and Fe_2O_3-nano mixed carbon electrodes were made into a pellet of 1 cm diameter. Cyclic voltammetry (CV) studies were carried out with a three-electrode glass cell assembly that had the Fe_2O_3-nano-loaded carbon or Fe_2O_3-nano mixed carbon electrode as the working electrode, silver oxide as the counter electrode, Hg/HgO (1 M NaOH) as the reference electrode and cellophane, together with filter paper, as the separator, which was sandwiched by the two electrodes. The electrolyte used was 8 mol dm^{-3} aqueous KOH. Cyclic voltammetry measurements were recorded at a sweep rate of 0.5 mV s^{-1} and in the range of −1.3 V to −0.1 V. After the fifteenth redox cycle, the Fe_2O_3-nano-loaded carbon and Fe_2O_3-nano mixed carbon electrodes were removed, washed with deionized water, dried and observed by SEM-EDS so as to compare with the results of the electrodes before cycling.

3. Result and discussion

The X-ray patterns of the Fe_2O_3-load AB and Fe_2O_3-loaded tubular CNF electrodes before and after the 15th cycle at different weight ratios of iron and carbon are presented in Fig. 2. It can be seen that for the Fe_2O_3-loaded carbon materials before cycling (Fig. 2a) at different weight ratios of iron and carbon, Fe_2O_3 is indeed present on the carbon surface. Therefore, the active material of the Fe_2O_3-loaded carbon materials is Fe_2O_3.

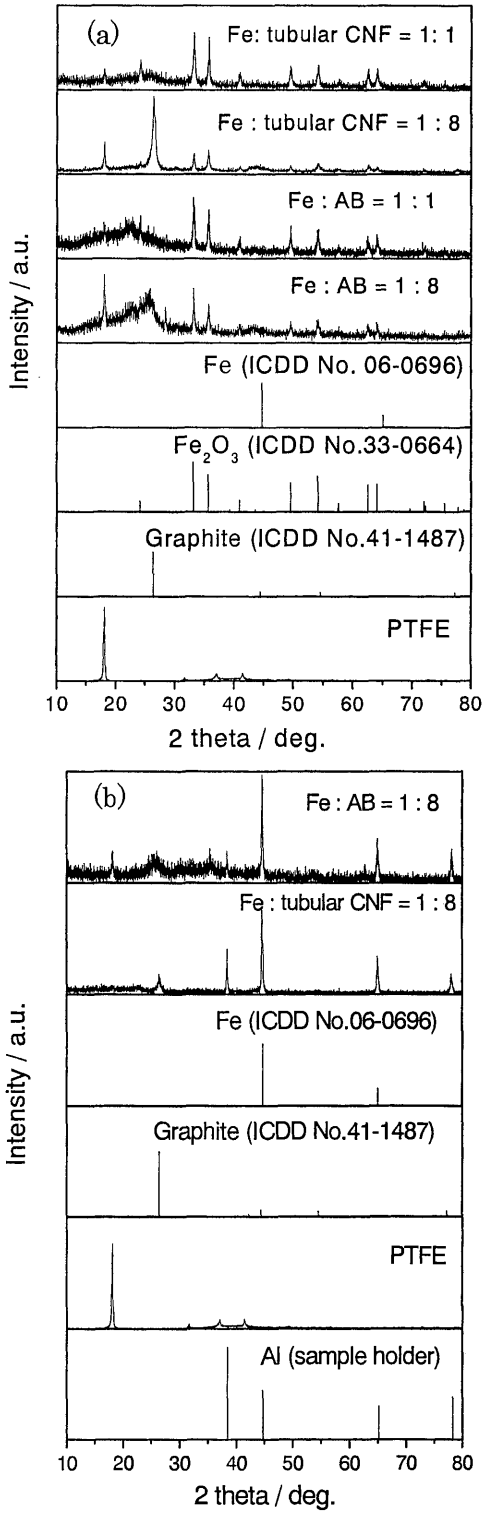

Fig. 2 X-ray pattern of Fe_2O_3-loaded AB and Fe_2O_3-loaded tubular CNF before (a) and after (b) cycling for different weight ratios of iron to carbon.

In order to confirm the nature of the Fe_2O_3 present on the carbons, TEM measurements were carried out. TEM images of as-prepared

Fe_2O_3-loaded carbons are shown in Fig. 3. The dark particles in this figure are Fe_2O_3. The TEM images demonstrated that fine Fe_2O_3 particles, tens of nanometers, were dispersed on the carbon surface and are hereafter referred to as "Fe_2O_3-nano-loaded carbon". Such a distribution of Fe_2O_3-nano is expected to improve the cycleability of the Fe_2O_3-nano-loaded carbon electrodes during cycling. However, the size of Fe_2O_3-nano particles in this case is larger than Fe_2O_3-nano powder (Aldrich) results in smaller surface area of Fe_2O_3-nano-loaded carbon electrodes than that of Fe_2O_3-nano-mixed carbon electrodes.

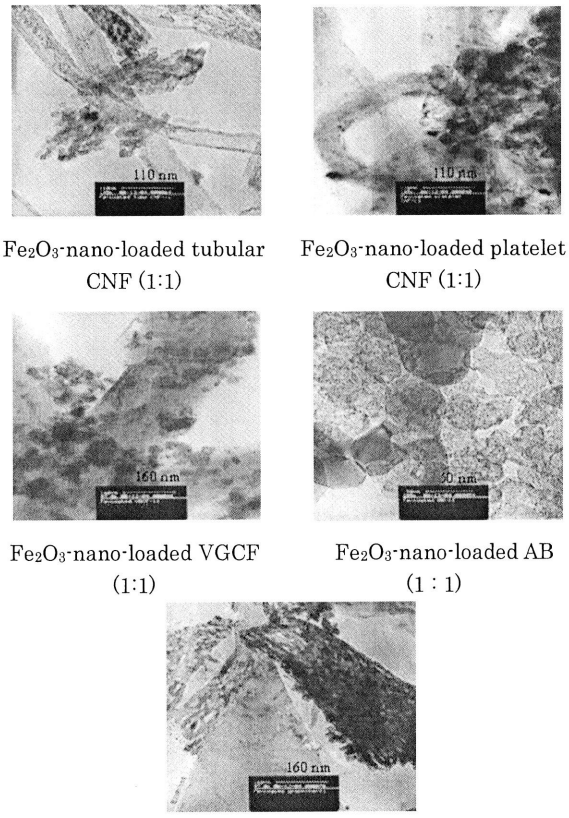

Fe_2O_3-nano-loaded tubular CNF (1:1)

Fe_2O_3-nano-loaded platelet CNF (1:1)

Fe_2O_3-nano-loaded VGCF (1:1)

Fe_2O_3-nano-loaded AB (1 : 1)

Fe_2O_3-nano-loaded graphite (1:1)

Fig. 3 TEM images of the as-prepared Fe_2O_3-nano-loaded carbon materials.

Figures 4-5 depict the SEM images and distribution of Fe_2O_3-nano and carbon particles by EDS of as-prepared Fe_2O_3-nano-loaded carbons and Fe_2O_3-nano mixed carbons with tubular CNF, AB and graphite, respectively. The distribution of Fe_2O_3-nano and carbon on both Fe_2O_3-nano-loaded carbons and Fe_2O_3-nano mixed carbons revealed that Fe_2O_3-nano was well dispersed on the carbon surface. Such dispersion should increase the active material surface area and improve the redox reaction of iron. Consequently, these electrodes are expected to provide large capacity.

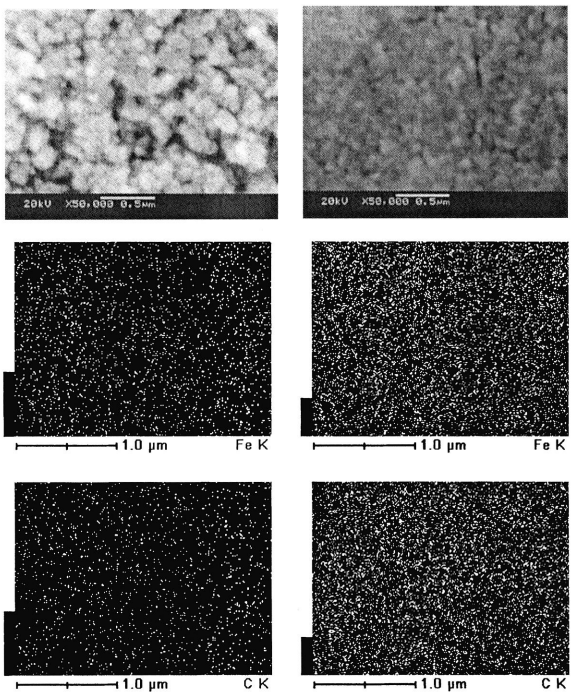

Fig. 4 SEM images and distribution of Fe_2O_3 and carbon of (a) Fe_2O_3-nano-loaded AB and (b) Fe_2O_3-nano mixed AB electrodes before cycle.

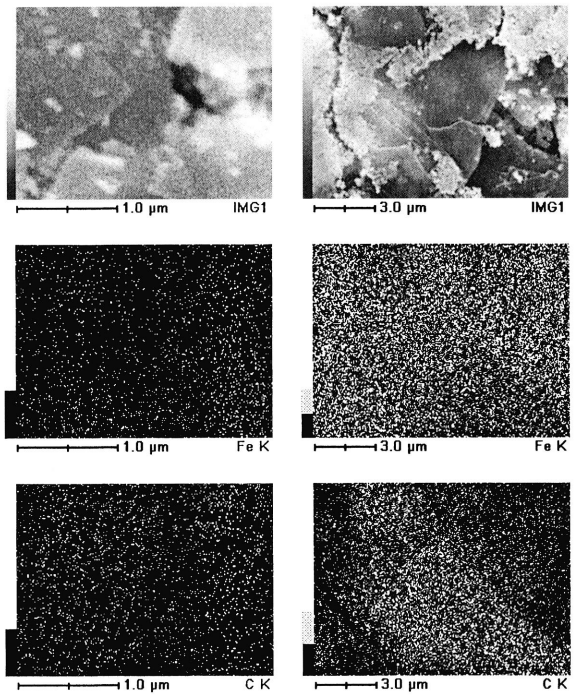

Fig. 5 SEM images and distribution of Fe_2O_3 and carbon of (a) Fe_2O_3-nano-loaded graphite and (b) Fe_2O_3-nano mixed graphite electrodes before cycle.

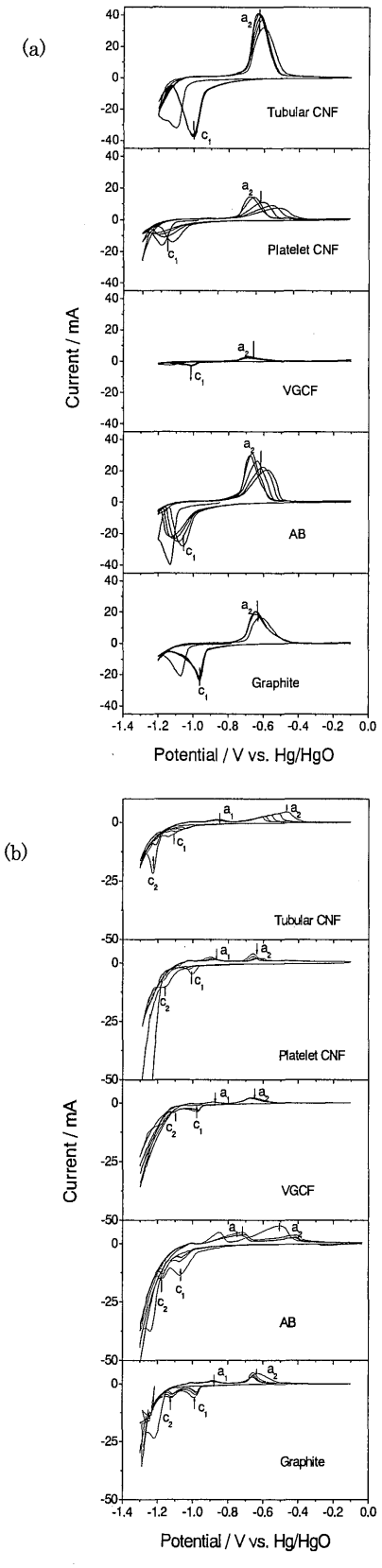

Fig. 6 Cyclic voltammetry of (a) Fe_2O_3-nano-loaded carbon (Fe:C:PTFE = 10:80:10 wt.%) and (b) Fe_2O_3-nano mixed carbon (Fe_2O_3:C:PTFE = 10:80:10 wt.%) electrodes. (arrows present the tendency of the current during the cycling).

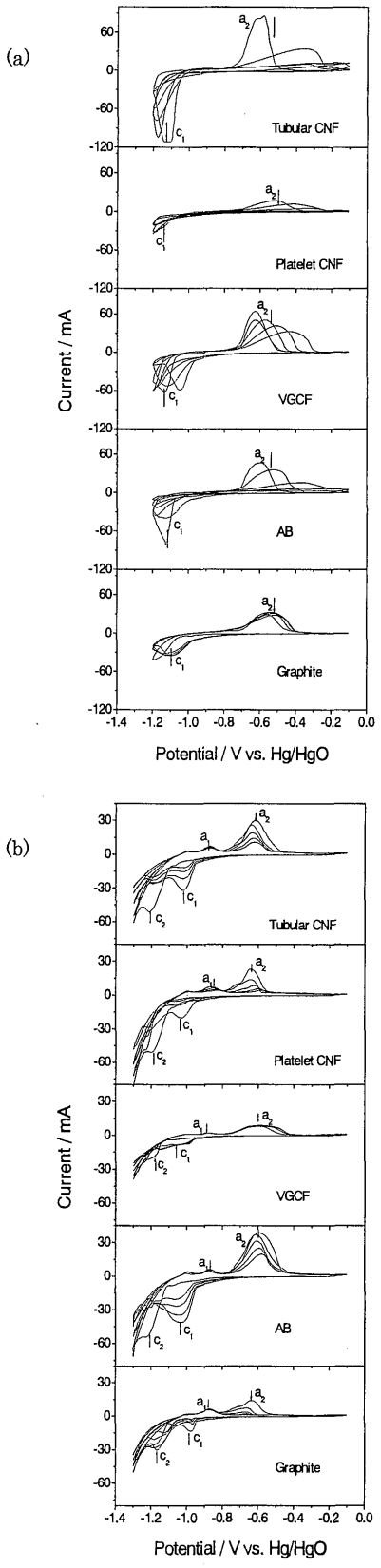

Fig. 7 Cyclic voltammetry of (a) Fe_2O_3-nano-loaded carbon (Fe:C:PTFE = 45:45:10 wt.%) and (b) Fe_2O_3-nano mixed carbon (Fe_2O_3:C:PTFE = 45:45:10 wt.%) electrodes. (arrows present the tendency of the current during the cycling).

Among carbon used for both kinds of materials, Fe_2O_3-nano-loaded and Fe_2O_3-nano mixed carbons, nano-carbons, based on large surface area, such as tubular CNF, platelet CNF, AB showed the more distribution of Fe_2O_3-nano on their surface than on VGCF or graphite.

The CV profiles of the Fe_2O_3-nano-loaded carbon electrodes having weight ratios of iron to carbon of 1:1 and 1:8 and Fe_2O_3-nano mixed carbon electrodes having weight ratios of Fe_2O_3 to carbon of 1:1 and 1:8 during the initial five cycles are shown in Figs. 6-7.

It is clearly that the preparative method for material affects on the redox behavior of electrode. In the case of Fe_2O_3-nano mixed carbon electrodes, for both two components (Fig. 6b, 7b), Fe/Fe(II) (eqn. 1) and Fe(II)/Fe(III) (eqn. 6 and/or 7) redox couples were observable. The Fe/Fe(II) couple (eqn. 1) was observed around -0.9 V on the oxidation and around -1.2 V on the reduction, respectively, while Fe(II)/Fe(III) (eqn. 6 and/or 7) appeared around – 0.6V and -1.0 V, respectively. However, the redox current for the Fe/Fe(II) couple was much smaller than that of the Fe(II)/Fe(III) couple. Consecutive cycling reduces the redox current under these peak couples. It suggests that the passivation of electrode was formed during cycling. For the Fe_2O_3-nano-loaded carbon electrodes (Fig. 6a, 7a), several peaks were observed, including the oxidation of Fe(II)/Fe(III) (eqn. 6 and or 7) at around –0.6 V and the corresponding reduction peak at around –1.1 V. With further cycling, the anodic peak moved to a more positive potential, while the cathodic peak shifted toward a more negative potential, and the current under these peaks decreased. This suggests that the reaction was becoming irreversible, resulting in increased overpotential. The redox couple of Fe/Fe(II) (eqn. 1) was not observable. This could be ascribed to the insulating nature of the $Fe(OH)_2$ active material, which would inhibit the Fe/Fe(II) redox couple, causing a large overpotential. $Fe(OH)_2$ will be reduced to Fe at a lower potential than the cutoff potential of -1.2 V. The other possible reason is hydrogen evolution, occurring at around -1.1 V. In the first cycle, Fe_2O_3 was reduced to $Fe(OH)_2$ and then $Fe(OH)_2$ was oxidized to FeOOH or/and Fe_3O_4; with further cycling, this Fe(II)/Fe(III) redox couple (eqn. 6 and or 7) became predominant, while the Fe/Fe(II) redox couple (eqn. 1) was insignificant.

In order to check the presence of the Fe/Fe(II) redox couple, CV measurements were carried out on Fe_2O_3-nano-loaded carbon electrodes with a reversal potential of -1.3 V (Fig. 8); after the 15th cycle, the cathodic scan from -0.1 to -1.3 V was stopped at zero current in the potential range – 1.1 to -0.9 V, and X-ray measurement wwas made. The XRD patterns of the Fe_2O_3-nano-loaded AB and Fe_2O_3-nano-loaded tubular CNF are shown in Fig. 2b.

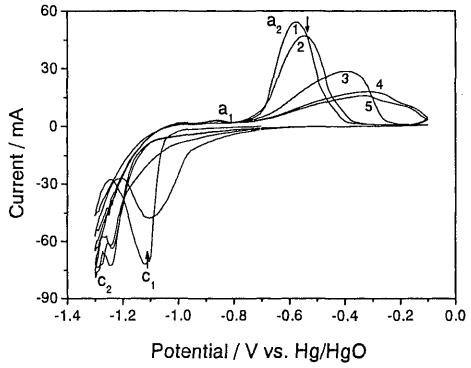

Fig. 8 Cyclic voltammetry of Fe_2O_3-nano-loaded AB (Fe:AB:PTFE = 45:45:10 wt.%) electrodes. (arrows present the tendency of the current during the cycling).

Figure 8 indicates that the Fe/Fe(II) oxidation peak (eqn. 1) occurred during the cycling around -0.9 V with much smaller current compared with that of Fe(II)/Fe(III) (eqn. 6 and/or 7) oxidation peak. The reduction peak of iron deposition was not separated from the hydrogen evolution peak. From Fig. 2b, it can be seen that Fe peaks are present on the carbon surface, thereby confirming that the Fe/Fe(II) redox process occurred during the cycling. However, Fe/Fe(II) couple was not observed on further cycling, and this may be due to the insulating nature of $Fe(OH)_2$. This was demonstrated clearly on the CV profile of Fe_2O_3-nano mixed carbon electrode (Fig. 6b, 7b). Although both Fe/Fe(II) and Fe(II)/Fe(III) redox couples were observed for Fe_2O_3-nano mixed carbon electrode, however, the redox current for the Fe/Fe(II) couple was much smaller than that of the Fe(II)/Fe(III) couple. Furthermore, the reduction peak of iron deposition occurred at a low potential (around -1.2 V) together with hydrogen evolution. The redox current under these peaks were decrease with increasing the cycle. These results revealed that the Fe_2O_3-nano-loaded carbon electrodes had larger internal resistances than that of the Fe_2O_3-nano mixed carbon electrode, leading to the disappearance of the Fe/Fe(II) redox couple. The reason may be due to the different size of Fe_2O_3 particles in these both electrodes.

As is evident from Figs. 6-7, addition the effects of preparation method for electrode

material, the type of carbon used as well as the ratio of iron to carbon, affect the redox behavior of iron. It can be seen that for both Fe_2O_3-nano-loaded carbons and Fe_2O_3-nano mixed carbons, the component correspondence with iron or iron oxide to carbon of 1: 1 exhibits larger redox current than that of 1:8. However, the iron to carbon is 1:8 shows the better retention of redox current than 1: 1 ratio for Fe_2O_3-nano-loaded carbon materials. Contrast, in the case of Fe_2O_3-nano mixed carbons, both components of iron oxide to carbon of 1:1 and 1:8 exhibits the decrease rapidly in redox current with repeated cycling. It is interesting to note that the redox current of Fe_2O_3-nano-loaded carbons are much larger than that of Fe_2O_3-nano mixed carbons at respective ratio between iron and carbon. This may origin the better contact between Fe_2O_3 and carbon due to the chemical mechanism in Fe_2O_3-nano-loaded carbons than mechanical binder in Fe_2O_3-nano mixed carbons. Other interesting property was obtained that is the currents ascribed hydrogen evolution at around -1.2 V of Fe_2O_3-nano-loaded carbons are much smaller than that of Fe_2O_3-nano mixed carbons (Figs. 6-7). This is expected to improve the discharge capacity and charge efficiency of Fe_2O_3-nano-loaded carbons. The main reason may be due to Fe_2O_3-nano-loaded carbon electrodes has smaller surface area than that of Fe_2O_3-nano mixed carbons. Beside the effects from ratio of iron to carbon, as well as preparation method for electrode material, the type of carbon used strongly affects the redox behavior of iron. Comparison of all carbons employed for the preparation of Fe_2O_3-nano-loaded carbon and Fe_2O_3-nano mixed carbon electrodes indicates that the tubular CNF, AB and graphite exhibited larger currents than VGCF and platelet CNF.

For all carbons, the redox current gradually decreased with repeated cycling. When a large amount of Fe_2O_3 was loaded, for example, the ratio between iron or iron oxide and carbon were 1:1 (Fig. 7), the redox current decreased rapidly with increasing cycling. The decrease in redox current may be explained based on the $Fe(OH)_2$ layer formed during the cycles, resulting in passivation. When a larger amount of Fe_2O_3 was loaded on the carbon, the $Fe(OH)_2$ layer should be thicker, thereby resulting in a rapid decrease of the redox current on cycling. Additionally, the morphology of the carbon affects the redox behavior of the Fe_2O_3-nano-loaded carbon and Fe_2O_3-nano mixed carbon electrodes. When nano-carbons, such as tubular CNF, AB, were employed, they exhibit larger current than other carbons. In the case of Fe_2O_3-nano-loaded carbon, graphite provided large current at both 1:1 and 1:8 ratios, while VGCF showed large currents at high Fe_2O_3 loadings, viz., ratio of 1:1. This behavior is acceptable, looking from the viewpoint of nano-carbons, especially tubular CNF and AB, which have larger actual surface areas than other carbons (Table 1). Consequently, Fe_2O_3 was more dispersed on tubular CNF and AB than other carbons, and the thickness of the $Fe(OH)_2$ layer on tubular CNF and AB was also thinner than on other carbons. Such dispersion results in a larger active surface area for Fe_2O_3-nano-loaded tubular CNF and Fe_2O_3-nano-loaded AB electrodes than other Fe_2O_3-nano-loaded carbon electrodes, thereby supporting the redox reaction of iron. However, the redox current decreased, even in the case of Fe_2O_3-nano-loaded tubular CNF and Fe_2O_3-nano-loaded AB on repeated cycling. This may be due to a dissolution-deposition mechanism, which would result in an intermediate species, i.e., $HFeO_2^-$ [11, 29], to be re-distributed on the carbon surface. In order to confirm the distribution of iron on the carbon surface, SEM and EDS studies were carried out with Fe_2O_3-nano-loaded carbon and respective Fe_2O_3-nano mixed carbon after the 15^{th} cycle and the results are presented in Figs. 9-10. Comparing the SEM and EDS before cycling (Figs. 4-5), it is clear that after cycling, for both types of electrodes, the iron was aggregated into large particles on the carbon surface, and this could be the reason for the decrease of redox current on further cycling.

Comparison of cyclic voltammetric results of Fe_2O_3-nano-loaded carbon and Fe_2O_3-nano mixed carbon electrodes at corresponding ratios, for all of the carbons, indicates that Fe_2O_3-nano-loaded carbon electrodes exhibit larger redox current than that of Fe_2O_3-nano mixed carbon electrodes and the iron-to-carbon ratio of 1:8 appears to give excellent, long cycle life for Fe_2O_3-nano-loaded carbon materials. Fe_2O_3-nano-loaded carbon material is a potential candidate for iron/air battery anode.

4. Conclusion

The type of carbon used and the ratio between iron and carbon as well as preparation method of electrode material play important roles in determining the electrochemical properties of Fe_2O_3-nano-loaded carbon and Fe_2O_3-nano mixed carbon electrodes. Fe_2O_3-nano-loaded carbons provide larger redox current than Fe_2O_3-nano mixed carbon

electrodes at both components iron to carbon 1:1 and 1:8. Higher redox currents are obtained for both types of electrode materials

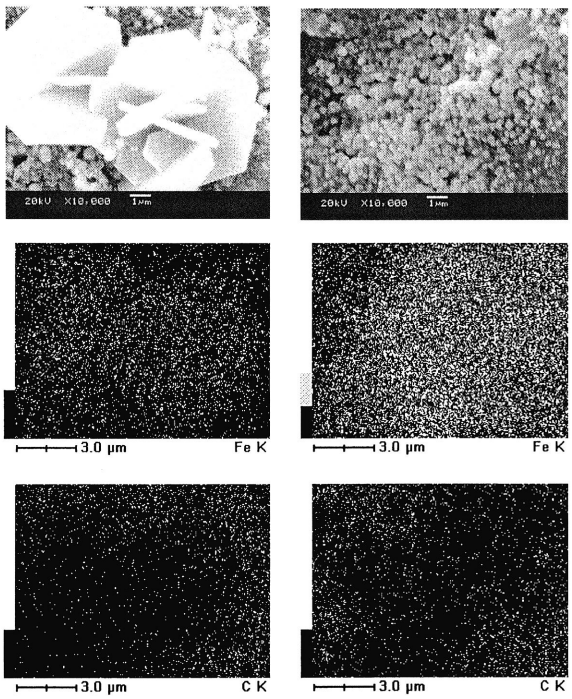

Fig. 9 SEM images and distribution of Fe_2O_3 and carbon of (a) Fe_2O_3-nano-loaded AB and (b) Fe_2O_3-nano mixed AB electrodes after the 15th redox cycle.

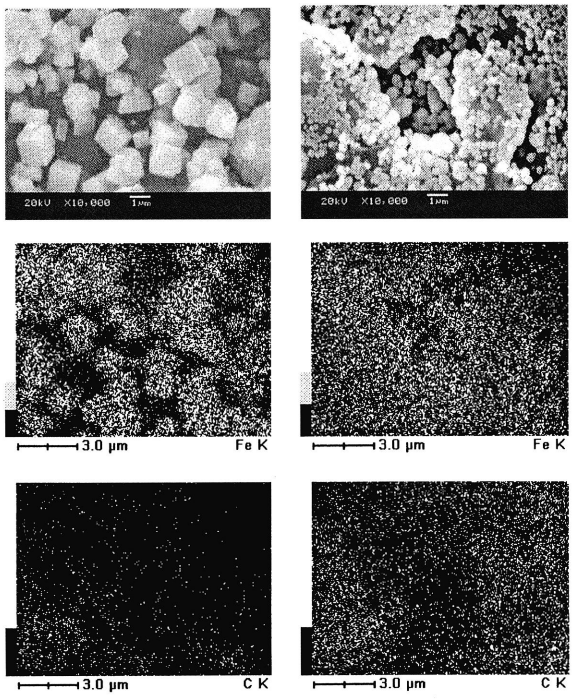

Fig. 10 SEM images and distribution of Fe_2O_3 and carbon of (a) Fe_2O_3-nano-loaded graphite and (b) Fe_2O_3-nano mixed graphite electrodes after the 15th redox cycle.

employing acetylene black and tubular CNF. The redox current decreased initially and stabilized after several charge/discharge cycles. The best performance for Fe_2O_3-nano-loaded carbon electrodes can be observed for an iron-carbon ratio of 1:8, in which tubular CNF, AB and graphite show the larger capacity than other carbons.

Comparison of Fe_2O_3-nano mixed carbon and Fe_2O_3-nano-loaded carbon electrodes indicates that higher capacities are obtained in the latter case due to the better contact between Fe_2O_3 and carbon based on the chemical incorporation than mechanical binder in Fe_2O_3-nano mixed carbon electrode.

Acknowledgement

This work was supported by the CREST program of JST (Japan Science & Technology Agency).

References

[1] L. Ojefors and L. Carlsson, *J. Power Sources*, 2 (1977/1978) 287-296.

[2] K. F. Blurtin and A. F. Sammells, *J. Power Sources*, 4 (1979) 263-279.

[3] A. M. Kannan and A. K. Shukla, *J. Power Sources*, 35 (1991) 113-121.

[4] K. Vijayamohanan, T. S. Balasubramanian and A. K. Shukla, *J. Power Sources,* 34 (1991) 269-285.

[5] C. Chakkaravarthy, P. Perasamy, S. Jegannathan and K. I. Vasu, *J. Power Sources,* 35 (1991) 21-35.

[6] M. Jayalakshmi, B. N. Begumi, V. R. Chidambaram, R. Sabapathi and V. S. Muralidharan, *J. Power Sources,* 39 (1992) 113-119.

[7] A. K. Shukla, M. K. Ravikumar and T. S. Balasubramanian, *J. Power Sources,* 51 (1994) 29-36.

[8] L. Ojefors, *J. Electrochem. Soc.*, 123 (1976), 824-828.

[9] Lars Ojefors, *J. Electrochem. Soc.*, 123 (1976), 1691-1696.

[10] R. S. Schrebler-Guzman, J. R. Viche and A. J. Arvia, *Electrochim. Acta*, 24 (1979), 395-403.

[11] G. P. Kalaignan, V. S. Muralidharan and K. I. Vasu, *J. Appl. Electrochem.*, 17 (1987), 1083-1092.

[12] K. Micka and Z. Zabransky, *J. Power Sources*, 19 (1987), 315-323.

[13] J. Cerny, *J. Power Sources*, 25 (1989), 111-122.

[14] P. Periasamy, B. R. Babu, S. V. Iyer, *J. Power Sources,* 58 (1996), 35-40.

[15] C. A. Caldas, M. C. Lopes. I. A. Carlos, *J. Power Sources*, 74 (1998), 108-112.

[16] C. A. C. Souza, I. A. Carlos, M. C. Lopes, G. A. Finazzi, M. R. H. de Almeida., *J. Power Sources*, 132 (2004), 288-290.

[17] B T. Hang., M. Egashira, I. Watanabe, S. Okada, J. Yamaki, S. Yoon and I. Mochida, *J. Power Sources,* In press (2005).